Index: amplifiers, communication satellites, degradation, intermodulation distortion, nonlinearity models

The IM Microscope: A new approach to nonlinear analysis of signals in satellite communications systems

D. S. ARNSTEIN, X. T. VUONG, C. B. COTNER, AND H. M. DARYANANI

(Manuscript received August 6, 1992)

Abstract

This paper describes a new technique, called the IM Microscope, for studying the effects of nonlinearities in satellite transponders. The approach is to first derive a least-squares solution for equivalent gain on each signal as it passes through the nonlinearity, and then to subtract the signals one by one from the output to obtain a residual intermodulation (intermod) noise waveform. The algorithm is first derived, and examples are then given of its use in calculating power density spectra and power division.

The IM Microscope can handle routine problems such as determining the carrier-to-intermod ratio of signals in a frequency-division multiple access (FDMA) transponder, and out-of-band emission levels for earth stations. This new approach does not become computation-bound when solving for high-order harmonic distortion such as passive intermod, or in situations with a large number of input signals. It can handle difficult cases, such as the intermod generated in a spread spectrum transponder, in an arbitrary nonlinear function, with a large number of unequal signals, or in computation of distortion with a time-dependent nonlinear device.

Introduction and background

A new technique called the IM Microscope has been developed at COMSAT for computing intermodulation (intermod) power spectra and nonlinear power division in satellite transponders, high-power amplifiers (HPAs), and other

nonlinear devices. It provides capabilities beyond those of current intermod analysis techniques, which date back to the early 1970s [1],[2]. For example, the following problems are difficult to solve using current nonlinear analytical approaches:

- Finding the spectrum of intermod and power division with overlapping spectra—a case which occurs with code-division multiple access (CDMA) or overlapping frequency-hopping multiple access (FH) signals.
- Inclusion of high orders of intermod products, such as passively generated intermod (PIM), in high-power satellites.
- The case of arbitrary nonlinear characteristics (*e.g.*, discontinuous, piecewise linear, defined by an analytical expression, or time-varying).
- Computing intermod from large numbers of unequal carriers.

Unlike synthesis techniques which build a model for intermod noise component-by-component (*e.g.*, third order, fifth order, *etc.*), the new approach works directly on composite simulated signals stored as a computer file. It strips away the wanted signal components one by one until a small residual intermod noise remains (hence the term "microscope").

Since its inception in 1990, the IM Microscope study at COMSAT has evolved through several stages. The software implementing the algorithm is designed to run on a 386-based personal computer (PC) with a math coprocessor. It is written in Lahey FORTRAN with DOS memory extension, and contains a variety of input signal models, including energy-dispersed carrier waves (ED/CWs), direct-sequence spread spectrum (DSSS) quadrature phase shift keying (QPSK) digital signals, bands of thermal noise, and unmodulated CWs. The IM Microscope played a key role in a Department of Defense-funded study [3],[4] testing the use of a voltage-controlled nonlinear function (time-varying nonlinearity) to enhance the antijam capability of a transponder.

This paper describes the new algorithm, discusses the rationale for development into its current form, and presents typical results.

Theory of operation

The IM Microscope is a two-step analysis procedure. With reference to Figure 1 (showing input signals $s_1, s_2, \ldots, s_L$ and output signals with equivalent gains, $\lambda_1, \lambda_2, \ldots, \lambda_L$), the procedure is as follows:

Step 1. Compute equivalent (stochastic) gains of all signals passing through the nonlinearity.

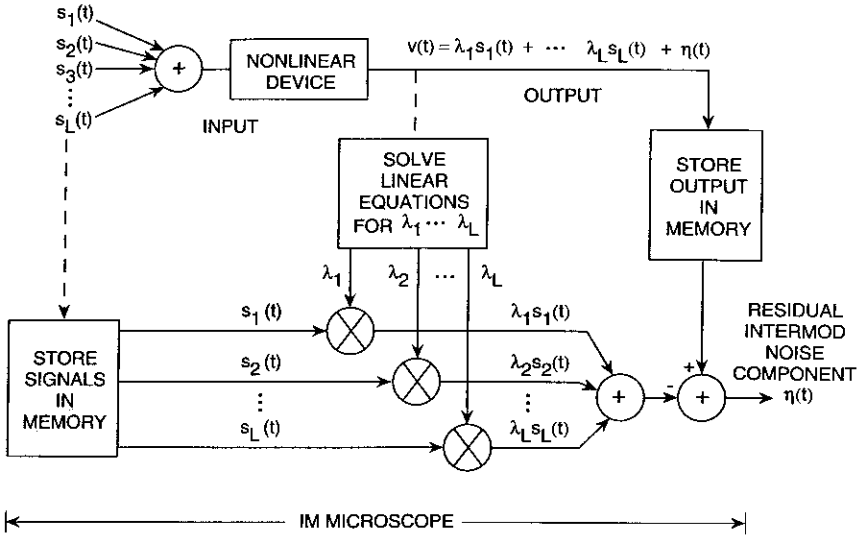

Figure 1. *Equivalent Gain and Residual Noise Model Forming the Basis of the IM Microscope*

Step 2. Subtract those signals from the output, leaving a residual which is the intermod noise.

Although this approach is intuitive, many problems had to be overcome to make it practical. A study program was initiated in 1990 by COMSAT World Systems (CWS) to test the feasibility of a software implementation of this procedure which was first suggested in 1979 [5].

The main problem encountered in carrying out step 1 is that, except for some simple nonlinearity problems with a few input signals, the closed-form analytical solution for equivalent gain produces intractable multidimensional integrals over the random variables that characterize the input signals. These integrals do not factor or otherwise simplify. For example, two independent signals in a transponder may be described in a vector space by a single random variable—the phase difference between the signals. Three signals could be characterized by two independent phase differences, and so on. Each time another independent signal is included, at least one more dimension is added to the integrals that must be solved to calculate a residual component. When

thermal noise and amplitude modulation signals are added to the collection of possible inputs, any hope of an analytical solution to steps 1 and 2 disappears.

A simulation approach which uses digital representations of the signals nicely sidesteps this dilemma, since a finite-time average can be computed directly from stored versions of computer-generated sample functions. Thus, a single variable (time) replaces the multitude of variables that would be needed to describe statistically independent signals, and a summation over the time variable replaces probability-based averaging. The IM Microscope, as realized in this study, is therefore a Monte Carlo-based approach that depends on accurately recreating digitally simulated versions of signals found in the transponder or other nonlinear device. The theoretical basis for the Monte Carlo approach is derived below, beginning with a narrowband representation of signals and associated bandpass nonlinearities.

Representation of narrowband signals

All signals in the IM Microscope are simulated with complex envelope representations of bandpass signals [6]. A bandpass signal occupies a restricted region of the frequency domain and can be represented by its (narrowband) in-phase and quadrature components, x_i and x_q, as

$$x(t) = x_i(t)\cos(\omega_o t) - x_q(t)\sin(\omega_o t) \qquad \text{[real signal]} \quad (1)$$

The real bandpass signal, $x(t)$, can be expressed as the real part of the product of the complex envelope component, $[x_i(t) + jx_q(t)]$, and the center frequency shift component, $e^{j\omega_o t}$. Calling $s(t)$ this product, we have

$$\begin{aligned} s(t) &= [x_i(t) + jx_q(t)]e^{j\omega_o t} \qquad \text{[complex signal]} \\ &= A(t)e^{jB(t)}e^{j\omega_o t} \end{aligned} \quad (2)$$

where

$$A(t) = \sqrt{x_i(t)^2 + x_q(t)^2}$$

and

$$B(t) = \arctan\left[\frac{x_q(t)}{x_i(t)}\right] \qquad \text{[four-quadrant arctan]}$$

Note that the original real signal can be recovered by taking the real part of the complex signal, as

$$x(t) = \text{Real}\{\text{complex envelope} \bullet e^{j\omega_o t}\} = \text{Real}\{s(t)\} \quad (3)$$

For purposes of calculation and computer representation, the complex envelope is better than the original signal because it consists entirely of low-pass functions, $A(t)$ and $B(t)$, making it easy to go from complex to real, and vice versa.

The IM Microscope represents all signals as sampled complex envelope signals. The sampling frequency, f_s, establishes a sampling interval, $\Delta t = 1/f_s$, and signals are represented at their nth time sample as

$$s(t = n\Delta t) = s(n) = [x_i(t = n\Delta t) + jx_q(t = n\Delta t)]\, e^{j\omega_o n\Delta t} \tag{4}$$

It is possible to move back and forth between the time and frequency representations of the signals by using the discrete Fourier transform (DFT), which is performed on a block of data consisting of N samples [7]. The coefficients of the DFT are

$$X(k) = \sum_{n=0}^{N-1} s(n) W_N^{kn} \qquad k = 0, 1, \ldots, N-1 \tag{5}$$

where $W_N = e^{j(2\pi/N)}$.

The quantity $X(k)$ represents the amplitude of a sinusoid at frequency $f_k = (k/N)(1/\Delta t) = kf_s/N$. From the N Fourier transform points, one then finds an approximate power spectral density function,

$$S(k) = X(k)X^*(k)/Nf_s = |X(k)|^2/(Nf_s) \qquad k = 0, 1, \ldots, N-1 \tag{6}$$

In the limit of large N, and after suitable normalization, the function $S(k)$ approximates the power spectral density of the signal.

If the time samples are separated by $1/f_s$ seconds, the frequency samples in a discrete complex Fourier transform are separated by f_s/N Hz. Thus, the width of the frequency window observed by the IM Microscope equals the sampling frequency, f_s, as sketched in Figure 2. The signals are placed within the window by the frequency-shifting function, $e^{j\omega_o n\Delta t}$. Signals are placed within the window to simulate carriers in a transponder.

Memory and run-time limitations caused by the DFT make it necessary to limit the block size, N. In the first working version of the IM Microscope program, N could be no larger than 2,048 samples. With a limit on block size, it then became necessary to average individual blocks of data to reduce the variance to an acceptable value, as follows:

$$\bar{S}(k) = \frac{1}{M} \sum_{m=1}^{M} S_m(k) \tag{7}$$

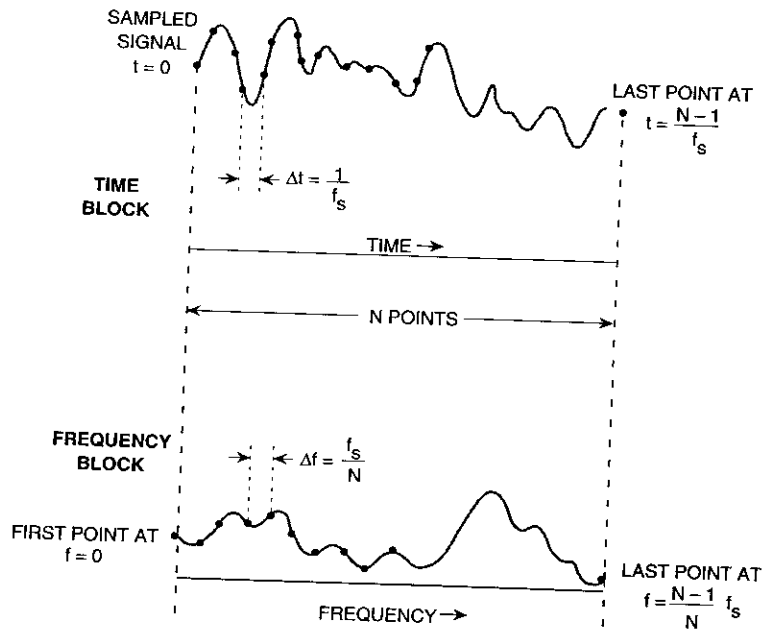

Figure 2. *Time and Frequency Windows of Data Blocks With Discrete Fourier Transform*

where M is the number of blocks of data, each with N points, and subscript m has been added to denote the spectrum from the mth block of data.

The spectrum of the complex samples of a bandpass signal "folds" or repeats with period f_s. With signal combinations near the middle of the window (*i.e.*, near $f_s/2$), folding takes place at the end-points, $k = 0$ and $N - 1$. *Aliasing* is a phenomenon that occurs when components of the signal being analyzed exceed the window end-points, causing the adjacent spectrum replications to enter the analysis window. To avoid aliasing in the IM Microscope, the input signals must be confined to a small portion of the total sampling window.

Representation of bandpass nonlinearities

A bandpass nonlinearity consists of three functional elements, as shown in Figure 3: a bandpass filter, a memoryless nonlinearity, and another bandpass (zonal) filter [8],[9]. In most satellite communications situations, signals are confined to a fairly narrow range of frequencies centered at f_0, so the first

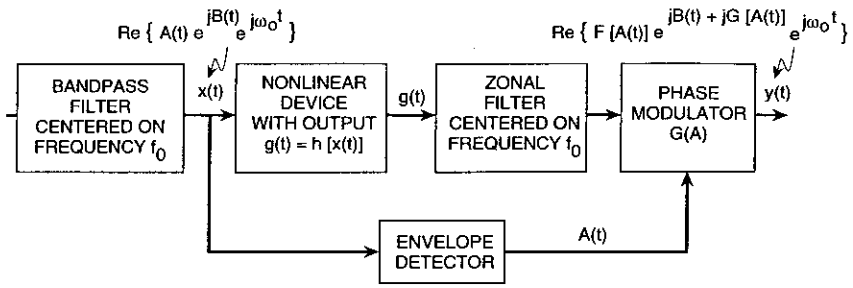

Notes:

1. x(t) is defined using equations (1), (2), and (3).
2. y(t) is defined in equation (8).
3. h ↔ F is a first-order Chebychev transform pair.
4. F(A) is the AM/AM distortion.
5. G(A) is the AM/PM distortion.
6. $\omega_o = 2\pi f_0$.

Figure 3. *Representation of a Bandpass Nonlinearity With Phase Shift*

bandpass filter is implicit. Similarly, because the output stage of a satellite (or earth terminal) amplifier is band-limited, the zonal filtering portion of the model is naturally present in most applications. This model is sufficient to explain so-called AM-to-AM types of nonlinear input/output characteristics. Because minor memory effects in high-power tubes or solid-state devices can have a major impact on the RF phase, a phase shifter is needed in the basic nonlinear model to account for these so-called AM-to-PM effects. The bandpass model, including phase shift, is described in References 1 and 10.

The IM Microscope combines the sampled data version of narrowband signals centered in the vicinity of f_0 with the nonlinear model shown in Figure 3. The nonlinearity acts on the RF signal input to create components at DC, f_0, $2f_0$, $3f_0$, *etc.*, while the final bandpass filter selects only the terms near frequency f_0. Calling $y(t)$ the real output of the final bandpass filter, $y(t)$ is given in terms of the input complex envelope variables $A(t)$, $B(t)$, and ω_o as

$$y(t) = \text{Re}\ \{F[A(t)]\, e^{jB(t)+jG[A(t)]}\, e^{j\omega_o t}\} \tag{8}$$

where $F(\bullet)$ is the first-order Chebychev transform of the RF nonlinearity $h(x)$. Note that $\omega_o = 2\pi f_0$. The function $F(\bullet)$ is an envelope nonlinearity embodying AM/AM distortion effects. The phase function, $G(\bullet)$, in the exponent is the AM/PM distortion.

The basic theory relating the RF nonlinear function, $h(\bullet)$, to the first zone function, $F(\bullet)$, is given in Reference 9. The IM Microscope user can select any nonlinear function, $F(\bullet)$, although in practice the function is usually obtained as a laboratory measurement relating the single-carrier input and output. The same can be said for $G(\bullet)$, which is normally the measured relative phase between input carrier and output carrier as a function of the input amplitude.

Equivalent gains and intermod noise

The basis for operation of the IM Microscope will be derived herein. With reference to Figures 1 and 3, the nonlinearity input can be written

$$s(t = n\Delta t) = s(n) = \sum_{i=1}^{L} s_i(n) \qquad n = 0, 1, \ldots, N-1 \qquad (9)$$

This sum is in turn expressible as a composite complex envelope signal,

$$s(n) = A(n)\, e^{jB(n)} \qquad n = 0, 1, \ldots, N-1 \qquad (10)$$

(Note that the frequency shift portion of the signal has been suppressed here for simplicity.) The post-nonlinearity complex bandpass envelope output, $v(t = n\Delta t) = v(n)$, with this input is given by

$$v(t = n\Delta t) = v(n) = F[A(n)]\, e^{jB(n) + jG[A(n)]} \qquad (11)$$

An equivalent representation is that each individual input, $s_i(n)$, passes through the nonlinearity essentially unchanged except for a fixed (but presently unknown) gain and phase shift. This complex gain can be designated λ_i, and is known as the equivalent gain.

When these signals are added together, along with their associated gains and phase shifts, they will not necessarily yield the observed output signal. Therefore, a residual signal $\eta(n)$ is needed as a correction. Thus, if L individual signals are summed, the output signal can be expressed as

$$v(n) = F[A(n)]\, e^{jB(n) + jG[A(n)]} = \sum_{i=1}^{L} \lambda_i s_i(n) + \eta(n) \qquad (12)$$

As it stands, this representation is incomplete because any L arbitrary values for the λ_i can be inserted, with the equation being satisfied by adjusting $\eta(n)$. Consequently, additional constraints must be placed on the gains and the residual. If the λ_i are considered as unknowns, they may be adjusted individu-

ally to make the cross correlation of $\eta(n)$ with each $s_i(n)$ equal to zero over the signal block (*i.e.*, for $t = n\Delta$ from $n = 1, 2, \ldots, N$).The function $\eta(n)$ takes on the meaning of a true uncorrelated residual function; that is, there is no part of $\eta(n)$ which will contribute to a correlation receiver searching for $s_i(n)$. The function $\eta(n)$ then becomes identical to intermod noise as defined in the literature—namely, a component orthogonal to all input signal components.

The above objective is achieved by taking the cross correlation of each signal, $s_i(n)$, with the noise waveform $\eta(n)$ and equating them individually to zero. Begin by solving for $\eta(n)$ in terms of the nonlinear output and input signals, using equation (12):

$$\eta(n) = v(n) - \sum_{i=1}^{L} \lambda_i s_i(n) \tag{13}$$

The cross correlation of $\eta(n)$ with $s_j(n)$ over a block of data is equal to the inner product of $\eta(n)$ with s_j^* (complex conjugate), which is then set to zero. Carrying out the cross correlation yields a set of L simultaneous equations, as

$$\sum_{n=0}^{N-1} \eta(n)s_j^*(n) = \sum_{n=0}^{N-1} v(n)s_j^*(n) - \sum_{n=0}^{N-1} \sum_{i=1}^{L} \lambda_i s_i(n)s_j^*(n) = 0 \qquad j = 1, \ldots, L \tag{14}$$

After interchanging the order of summation, the set of L equations in the L unknowns $\lambda_1, \lambda_2, \ldots, \lambda_L$ can be written

$$\mathbf{H}\boldsymbol{\lambda} = \mathbf{w} \tag{15}$$

where $\mathbf{H}$ is a positive definite Hermitian matrix of cross correlation values,

$$h_{ij} = \sum_{n=0}^{N-1} s_i(n)s_j^*(n) \tag{16}$$

$\mathbf{w}$ is the vector of output correlations

$$w_i = \sum_{n=0}^{N-1} v(n)s_i^*(n) \tag{17}$$

and $\boldsymbol{\lambda}$ is the vector $[\lambda_1 \ldots \lambda_L]^T$.

The solution to equation (17) is the set of desired equivalent gains. When a solution exists, it is unique. If a solution does not exist, it means that one or more of the original input signals is a linear combination of the others, so the

dimensionality needs to be reduced. In a practical communications setting, this condition should not occur.

Note that since the matrix **H** is positive definite and Hermitian, the solution to equation (15) can most effectively be obtained by the Cholesky decomposition method [11], where **H** is decomposed into a product of a lower triangular matrix, **L**, and its conjugate transpose $\mathbf{L}^{*T}$, as

$$H = \mathbf{L}\mathbf{L}^{*T} \tag{18}$$

and the solution to equation (15) can be obtained by solving the following two linear equations by substitution:

$$\mathbf{L}y = \mathbf{w} \tag{19}$$

$$\mathbf{L}^{*T}\boldsymbol{\lambda} = y \tag{20}$$

In the IM Microscope, **H** has the additional property of being almost diagonal; that is, the off-diagonal terms are usually very small compared to the diagonal terms since the input signals will tend to have very low cross correlation. As the block size approaches infinity, the cross correlations will tend to zero as a fraction of the total; however, for any finite simulation block size, the residual cross correlations, while small, must be taken into account in order to accurately represent the phase and amplitudes of the equivalent gains. In solving equation (15) using equations (19) and (20), the IM Microscope takes into account off-diagonal terms.

The solution of equation (15) represents Step 1 referred to in the introduction to this section. Substitution of the solution for $\boldsymbol{\lambda}$ into equation (13) represents Step 2.

The reason for using Monte Carlo or time-based averaging to derive **H** and **w** should now be clear. In a closed-form analytical solution of the simultaneous equations, having $(L - 1)$ independent phase separations plus other statistical descriptors for each input signal, computation of each term in **w** would require a minimum of an $(L - 1)$ dimensional integration. However, the Monte Carlo approach requires only a one-dimensional summation over the time variable, n. This task is easily carried out in a computer simulation where the waveforms are generated and stored in files.

The introduction to Reference 5 gives some historical background on the use of equivalent gains in solving nonlinear problems, while Reference 12 presents a stochastic decomposition approach that was applied to frequency-division multiplex (FDM) signals. Others [13] have used equivalent gains to obtain closed-form expressions for signal-to-total-noise ratio after the nonlinearity. The use of equivalent gains presented here is novel in that it is

embedded in a purely Monte Carlo simulation, allowing a broad category of signal and nonlinearity types to be represented.

Examples and applications

It was anticipated early in the study that most users of an intermod calculator would want to see a power spectrum plot. Hence, a significant effort was directed toward providing graphical output. This section describes the generation of a class of signals that can represent a transponder's frequency plan.

Rectangular spectrum inputs

The first working version of the IM Microscope used FDM signals having rectangular signal spectra. This signal set is referred to as ED/CW. The IM Microscope generates a rectangular spectrum by frequency-modulating a carrier with a triangular waveform, as shown in Figure 4. The principle involved is that, for a sufficiently large modulation index, the spectrum of an FM signal approximates the probability density of the frequency modulation [14]. Thus in principle any spectrum shape can be created by properly frequency-modulating a carrier. The modulating frequencies are chosen to yield high modulation index FM, and the triangular start time and its frequency are randomized.

If the triangular frequency functions were not randomized, the intermod spectrum would be based on signals that were not statistically independent (even though they had close to zero cross correlation), and therefore would not contain all the spectral components normally found by analytical approaches. This fact, which was discovered early in the study, is important in applying a Monte Carlo approach. For example, if multiple QPSK DSSS signals are used, but they are all *in bit sync* (a situation that could exist in an earth station where all modems are synchronized to the same source), the intermod spectrum will appear very different than if the signals have a randomized bit sync. In the first case, the intermod products will themselves be QPSK, and hence the same bandwidth as the original signals. In the latter case, the products will be modulated by the out-of-sync condition of their respective components, thereby spreading the bandwidth. This is the same spreading that normally occurs via the convolution operation in analytical approaches. The discovery that intermod products do not necessarily convolve, or spread, if the input signals are not statistically independent necessitated efforts to ensure the randomizing of all input signals in the IM Microscope (see Figure 14).

The complex FM signal, $s_i(t)$, centered at frequency f_i [generated as shown in Figure 4 from a triangular sweep function, $f(t)$], can be written

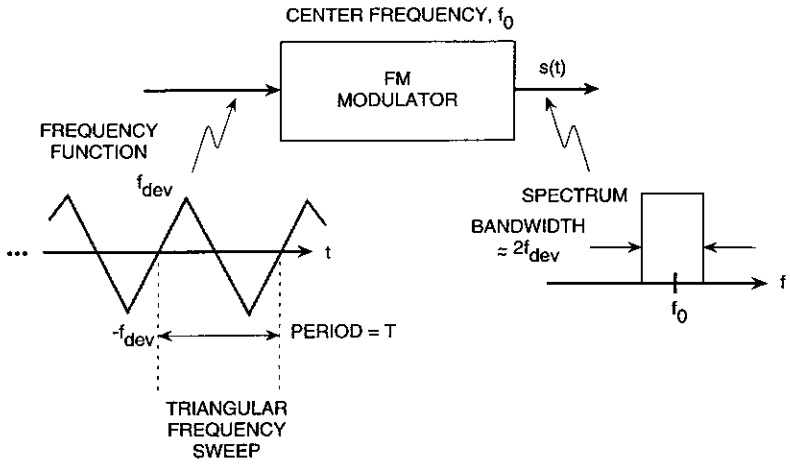

(a) Signal Generator Module for Energy-Dispersed CW

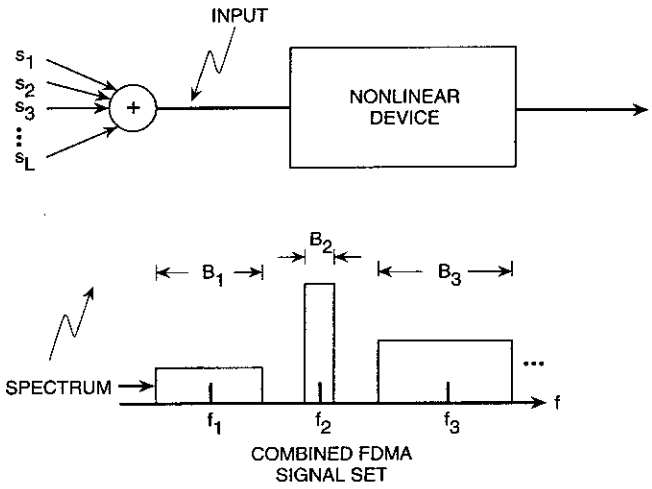

(b) Composite Input Signal Model

Figure 4. *Rectangular Spectrum Signal Generation Module*

$$s_i(t) = a_i e^{j\Phi(t)} e^{j2\pi f_i t} \tag{21}$$

where $\Phi(t)$ is the integral of the instantaneous radian frequency function $\omega(t) = 2\pi f(t)$, with $f(t)$ the triangular sweep function and a_i a constant that fixes the amplitude of the signal. Expanding the triangular function of Figure 4 in terms of a Fourier series gives

$$f(t) = 2f_{\text{dev}} \sum_{k \text{ odd}} (2/k\pi)^2 \cos(k2\pi f_r t) \tag{22}$$

where the repetition frequency, f_r, is equal to $1/T$, with T being the period. Thus, after integration of the frequency function, the phase function, $\Phi(t)$, is given by

$$\begin{aligned}\Phi(t) &= \int_0^t 2\pi f(t)\,dt \\ &= \frac{8}{\pi^2}\frac{f_{\text{dev}}}{f_r} \sum_{k \text{ odd}} \frac{1}{k^3} \sin(k2\pi f_r t)\end{aligned} \tag{23}$$

Representing the signal by its samples at $t = n\Delta t$, where, as before, Δt is equal to $1/f_s$, with f_s as the sampling rate [see also equation (14)], gives

$$s_i(n) = a_i e^{j\Phi(n\Delta t)} e^{j2\pi f_i n\Delta t} \tag{24}$$

The FM modulation index is the ratio f_{dev}/f_r, while the bandwidth of $s(t)$, B, is given approximately by Carson's rule,

$$\begin{aligned}B &\cong 2(f_{\text{dev}} + f_r) \\ &\approx 2f_{\text{dev}} \qquad \text{if } f_r << f_{\text{dev}}\end{aligned} \tag{25}$$

Then, the number of cycles of the sweep function in a data block of size N is given by

$$\begin{aligned}\text{No. cycles per block} &= \frac{\text{Total time in block}}{\text{Time per cycle of triangle}} \\ &= \frac{N}{f_s} \bullet \frac{1}{T} = \frac{f_r}{f_s} N\end{aligned} \tag{26}$$

Ideally, N should be very large, in order to make the number of cycles of the triangle in all signal blocks very large and thus obtain a good statistical averaging of the intermod. Since memory limitations have constrained the

block size (in an early version to $N = 2{,}048$), a previously described block-averaging approach is used in which the number of cycles per block is purposely set low—on the order of one to two cycles per block, or less—and multiple blocks of computed intermod are averaged.

In the program that was implemented, randomized triangular start times and incommensurate repetition rates are used, with the triangular sweep functions continuing uninterrupted from one block to the next. It was found experimentally that block counts of 10 to 100 times the number needed for a complete triangular period (reciprocal number of cycles per block) are required to create good statistical estimates of an intermod spectrum. Approximately 50 triangular repetitions were found to yield a good tradeoff between spectrum smoothing and run time.

Subsequently, additional signal sets were added, including the following:

- *QPSK DSSS.* Digital signal modulated by a pseudorandom bit sequence.
- *Filtered QPSK DSSS.* The same as QPSK, but band-limited.
- *Bandpass Thermal Noise.* Bands of noise derived by filtering white noise (independent Gaussian-distributed samples).
- *Bandpass Hard-Limited Thermal Noise.* A single band of thermal noise that is hard-limited to create a broadband constant envelope signal.

Examples of intermod spectra with these various signal combinations are given below.

Intermod spectra examples

Figure 5 illustrates a typical satellite transponder in which intermods are generated in the HPA. The input is four FDM signals, each having a specific center frequency, bandwidth, and input backoff relative to HPA saturation. Note that these ED/CW signals were randomized as described above, and multiple block averages were used to find the spectrum. The spectral plots in Figure 5 show information that is readily available with any direct observation of the input/output signals, through simulation or direct laboratory measurement. However, the ratio of signal-to-intermod noise density, or *C*/IM, at the point in frequency where the input signal is located is not available in these two plots.

The IM Microscope can now be applied to obtain the intermod spectrum shown in Figure 6. The four signals are spaced with a frequency plan that was chosen to be free of third-order intermods at the points where the input signals

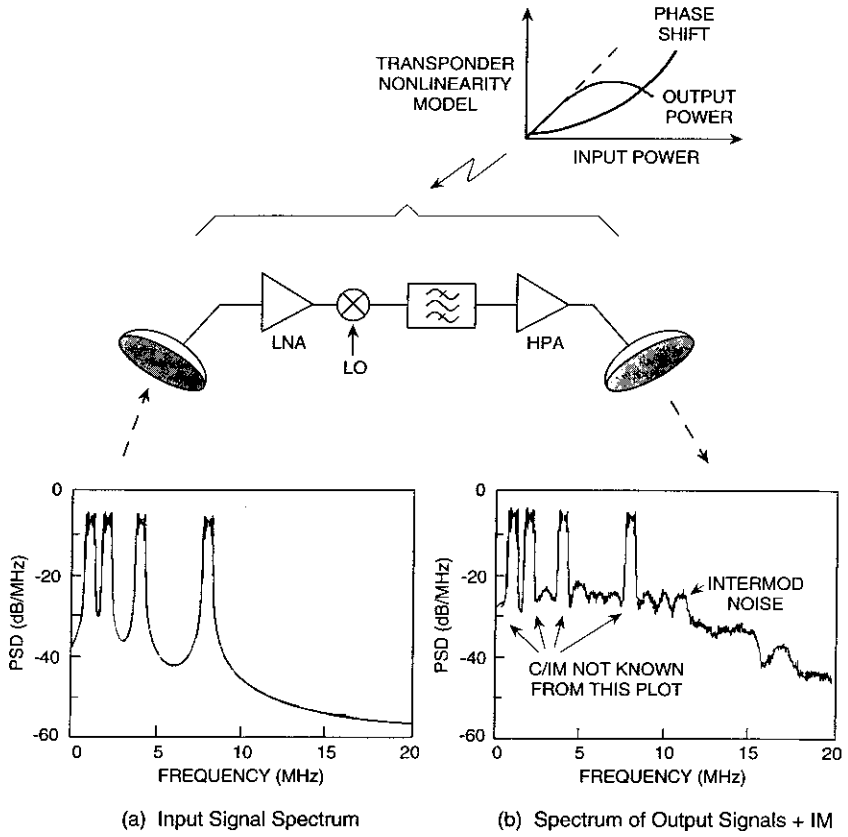

Figure 5. *Example of Transponder Loading With Equal Amplitude Signals and 3rd-Order IM-Free Spacing*

are located. (This is an example of a "1, 2, 4, 8" plan, where the number indicates the center frequency's location [here, in megahertz] relative to an arbitrary starting point of zero.) The design of plans that are free of third-order intermods is discussed in Reference 5. Since $\eta(t)$ does not contain any intermods of the form $2A - B$ or $A + B - C$ (see Reference 15 for explanation), there are dips in the spectrum at the signal center frequency locations, hidden by the signals in Figure 5. Therefore, the intermod that appears at these locations in Figure 6 consists of all remaining products (fifth order, seventh order, *etc.*). Many approaches have been developed to design and analyze intermod-free or

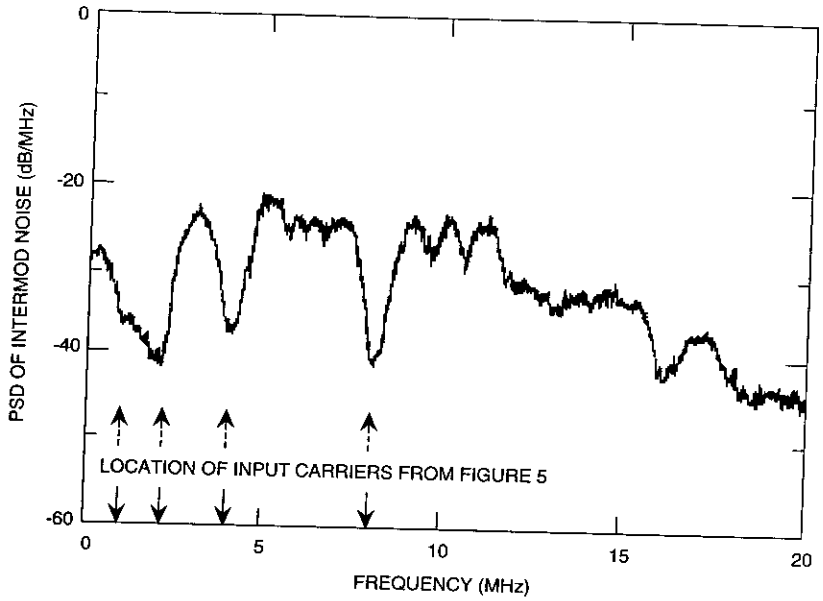

Figure 6. *IM-Only Spectrum With 3rd-Order IM-Free Carrier Plan*

low-intermod frequency plans [16], but all depend on the ability to compute the spectral level of intermod noise at the locations where the signals themselves are located.

Figures 7 and 8 give other examples of input/output spectra and associated intermod based on use of the IM Microscope. The signal model used in these figures is ED/CW. The nonlinear characteristic used in Figures 5 through 8 was a measured traveling wave tube amplifier (TWTA) AM/AM and AM/PM curve.

The IM Microscope can handle a wide variety of nonlinear characteristics. Figure 9 shows a few representative types. Any piecewise continuous or analytically expressible curve can be employed; there is no need to represent the characteristic in terms of a polynomial expansion.

Another limitation of previous techniques has been the need to group intermod products by "order" (*e.g.*, third order, fifth order, *etc.*). By computing the exact intermod waveform as a process of elimination, the IM Microscope is actually computing all harmonics of the intermod at once, to within the numerical accuracy permitted by the digital simulation. Figure 10 shows

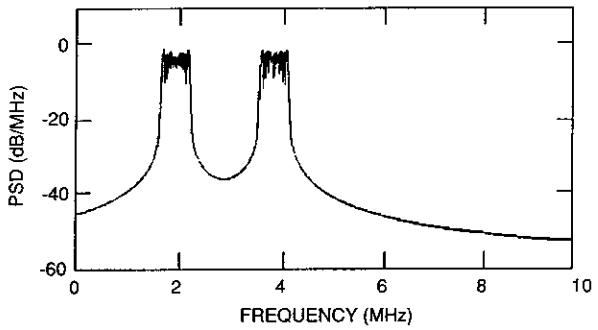

(a) Spectrum of Input Signals

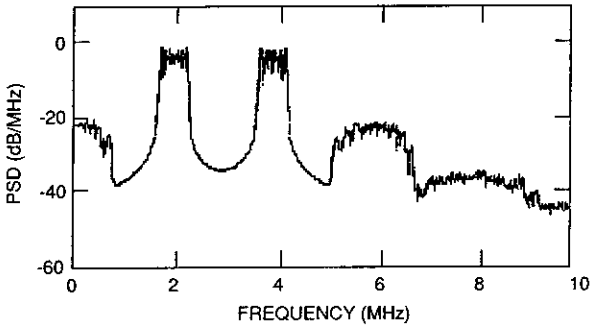

(b) Spectrum of Output Signals + IM

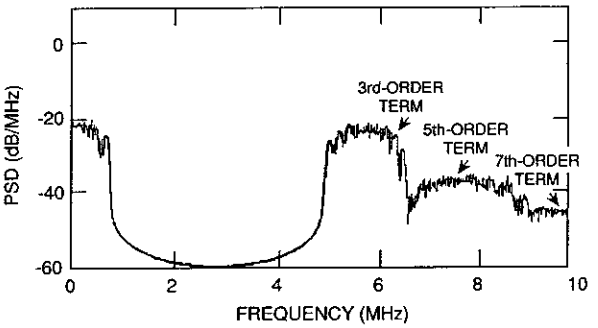

(c) Spectrum of IM Only

Figure 7. *Two-Carrier Frequency Plan Showing IM Generation Out-of-Band*

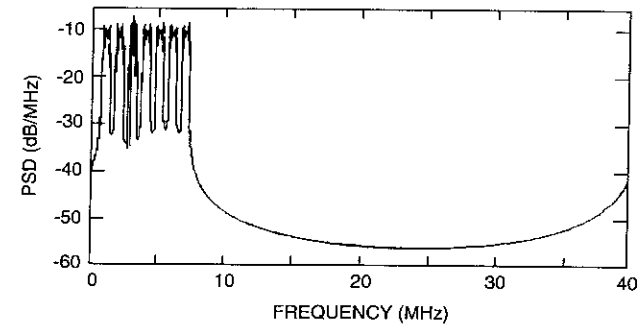

(a) Spectrum of Input Signals

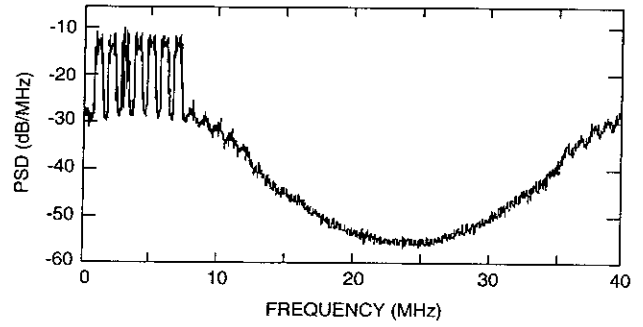

(b) Spectrum of Output Signals + IM

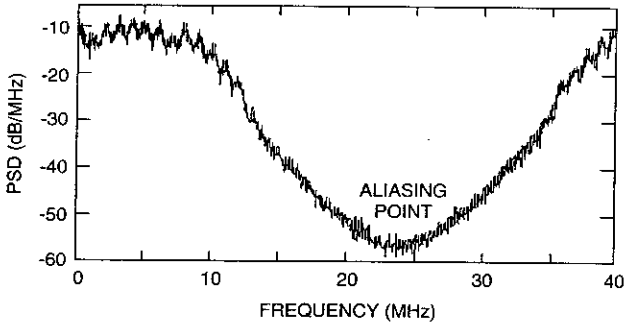

(c) Spectrum of IM Only

Figure 8. *Picket Fence Frequency Plan: Equal Size and Equal Spacing*

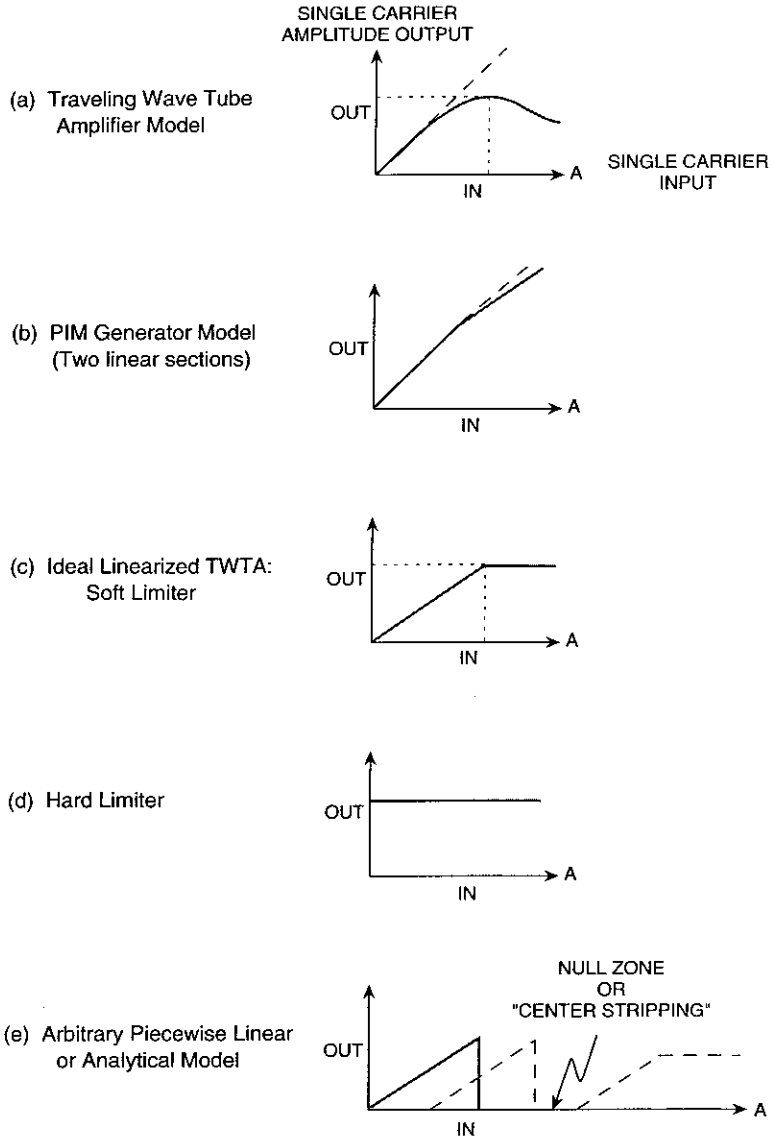

Figure 9. *Examples of AM/AM Characteristics Allowed With the IM Microscope*

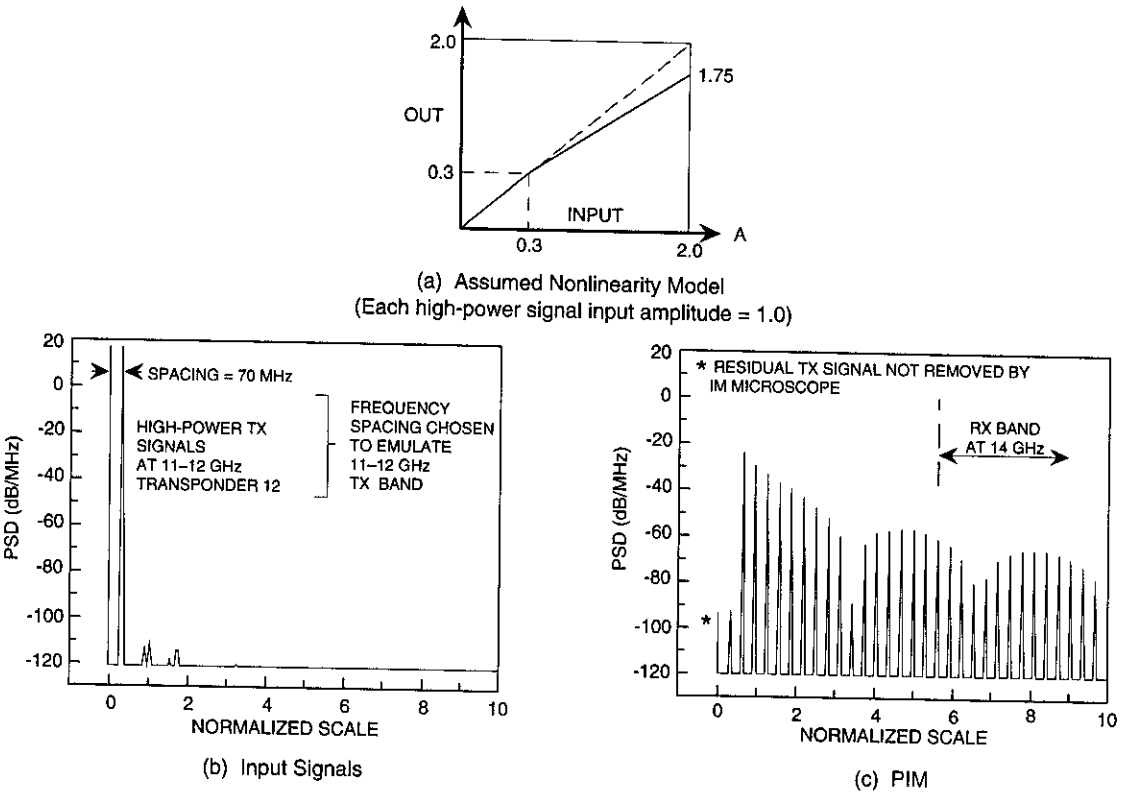

Figure 10. *Example of Passive IM Calculation With Nonlinearity Model Consisting of Two Linear Sections*

the spectrum for a hypothetical PIM nonlinearity model (given in the inset), showing the generation of very high orders of intermod originating from two CW signals. Two equal CW signals are illustrated being transmitted at the low end of the frequency scale through a hypothetical antenna system, with PIM components being generated in the receive band of the satellite's up-link at the upper end of the scale. As is usual in these cases, no filtering can take place once the signal leaves the antenna. Frequency spacings are chosen to simulate a Ku-band satellite. (It should be noted that an actual PIM nonlinearity would be much more subtle than that shown in Figure 10, and the frequency plan would be more complex than just two equal signals).

Note that by varying the breakpoint in the AM/AM characteristic, the PIM spectrum changes as shown in Figure 11. For the cases illustrated in Figures 10 and 11, where the intermod of interest is totally outside the transmit band, straight digital simulation could have been used as an alternative to the IM Microscope because subtraction of the input signals was not required. However, to see the effects of PIM in-band with wanted signals, or to see the actual time domain PIM waveform, the IM Microscope is necessary. Note that the IM Microscope could be used to find a nonlinearity that matches a given spectrum of a system under test. The nonlinearity shape might reveal the physical nature or source of the imperfection.

Figures 12 and 13 illustrate still other examples of the IM Microscope. In Figure 12, three bands of noise were chosen to simulate a network of spread spectrum users. Individual signals representing narrowband digital signals are added in the guard bands. The resulting intermod spectrum consists of discrete and continuous components. In Figure 13, a filtered QPSK signal is added to a large unmodulated CW signal (representing a jammer). The intermod spectrum is revealed as a series of discrete and continuous components.

Nonlinear power division and the IM Microscope

This discussion has thus far emphasized the spectrum of the intermod. In operations where there is a large disparity in input signal levels, the division of a nonlinearity's available RF power among those signals can be of primary interest. For example, in a transponder with one or two large FM/TV or QPSK/TDMA signals sharing the band with one or two small single-channel-per-carrier (SCPC) signals, both the division of power and the intermod spectrum are important. Another example is a military satellite with a single large hostile carrier attempting to jam a transponder filled with traffic.

In general, a large signal will capture power in an amplitude-limiting nonlinearity and suppress the smaller signals. For a center-stripping nonlinearity,

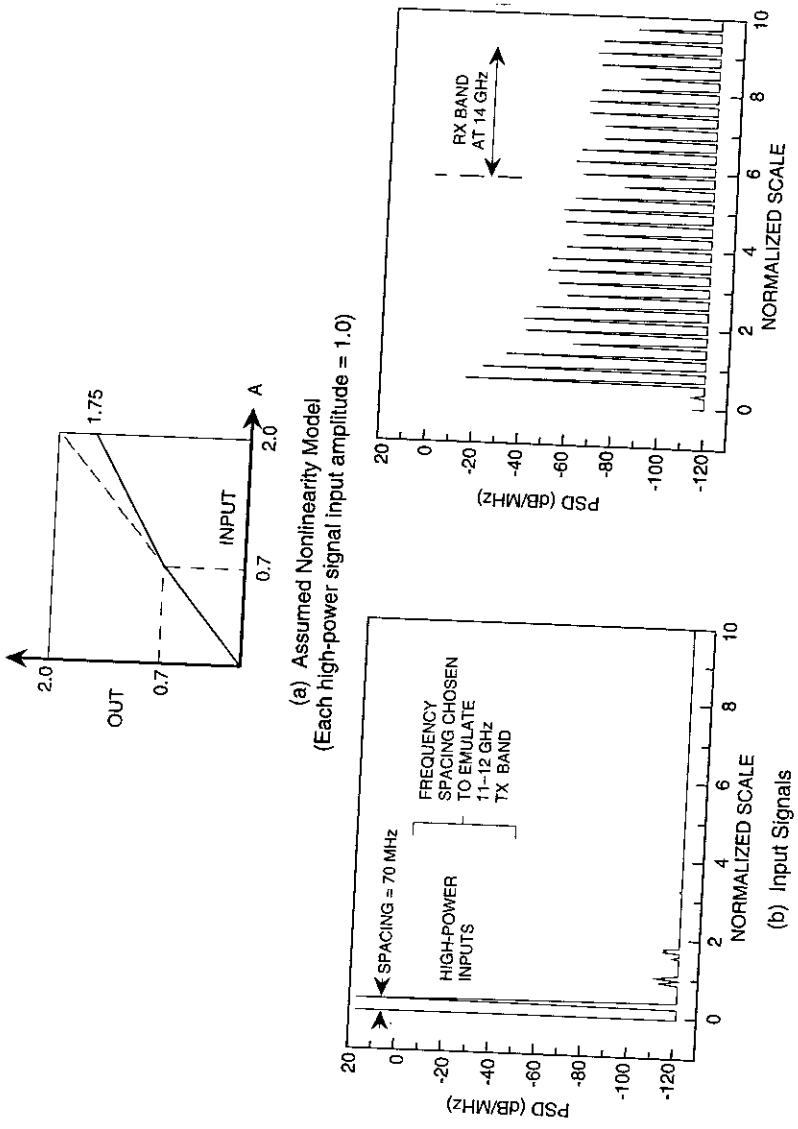

Figure 11. *Effect of Varying Two-Section Nonlinearity Model (from Figure 10) to Observe Changes in PIM*

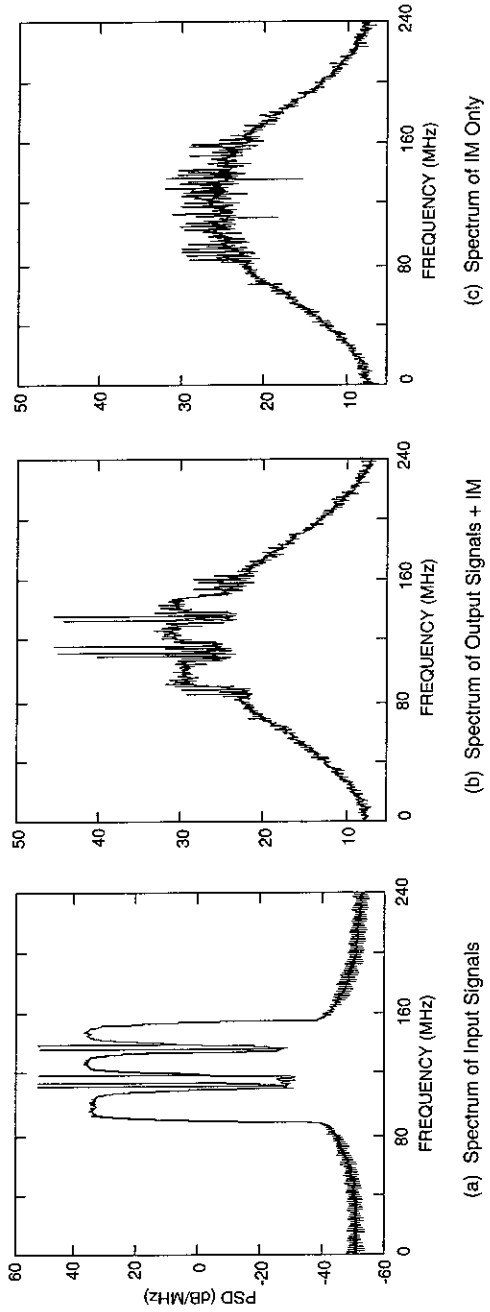

Figure 12. *Simulation of Network of Spread Spectrum Users and Unspread Digital Carriers (Thermal noise bands and CWs)*

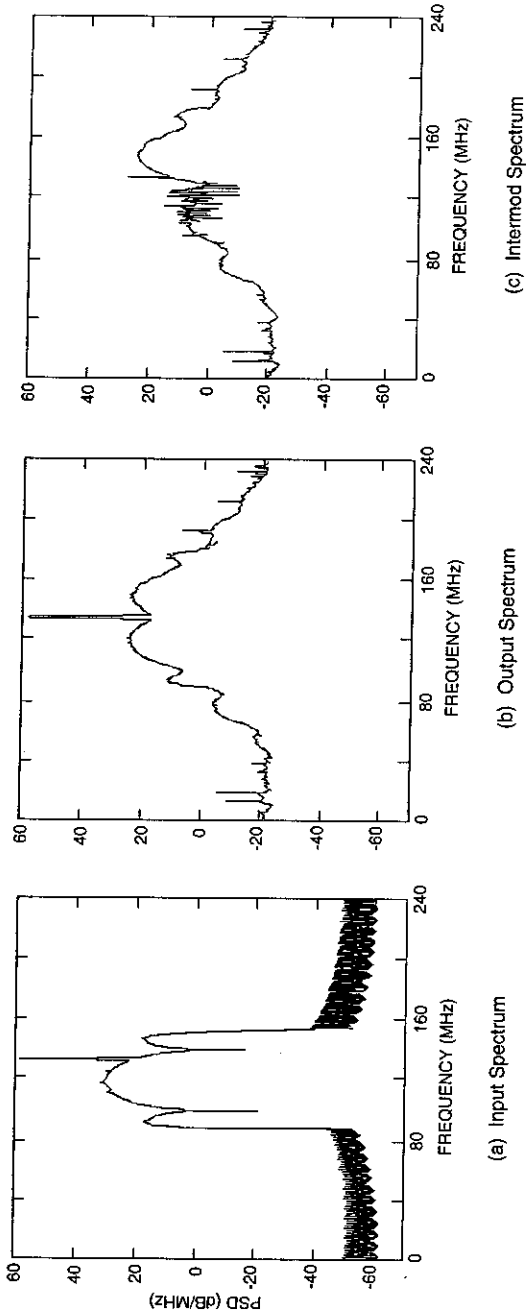

Figure 13. *40-Mbit/s QPSK DSSS Signal Plus CW Jammer in Hard Limiter (Input band-limited to 60 MHz)*

as defined in References 3 and 4 and illustrated in Figure 9e, the situation is reversed and a small signal can emerge *enhanced* relative to a larger jamming signal.

Unequal power division among the signals transiting the nonlinearity may be computed by finding appropriate equivalent gains. By suppressing the total time variable in a block of samples, the total energy of the signal can be used in place of the average power for convenience of calculation, as shown below. The total energies in the signals and intermod components can be expressed as follows:

$$\text{Input total energy} = \sum_{n=0}^{N-1} |s(n)|^2 = \sum_{i=1}^{L} \sum_{j=1}^{L} \sum_{n=0}^{N-1} s_i(n) s_j^*(n) = \mathbf{u}^T \mathbf{H}\, \mathbf{u} \quad (27)$$

$$\text{Output total energy} = \sum_{n=0}^{N-1} |v(n)|^2 = \boldsymbol{\lambda}^T \mathbf{H}\ \boldsymbol{\lambda}^* + \text{IM energy} \quad (28)$$

$$\text{IM energy} = \sum_{n=0}^{N-1} |\eta(n)|^2 \quad (29)$$

where $\mathbf{u}$ is the unit vector. Terms corresponding to the on-diagonal elements of matrix $\mathbf{H}$ in equations (27) and (28) are the computed energies in the signals at the input and output, respectively, as

$$i\text{th signal input energy} = \sum_{n=0}^{N-1} |s_i(n)|^2 \quad (30)$$

$$i\text{th signal output energy} = |\lambda_i|^2 \cdot \sum_{n=0}^{N-1} |s_i(n)|^2 \quad (31)$$

In a simulation the terms associated with the off-diagonal elements of $\mathbf{H}$ take negative and positive values that are small compared to those associated with the on-diagonal elements. For most practical applications, the power division can be accurately represented by equations (30) and (31), for $i = 1, 2, \ldots, L$.

An important example of the use of power division involves a transponder containing a hard limiter in the presence of jamming. The input is characterized by a certain power ratio, J/S, while the output ratio, $(J + \text{IM})/S$, determines the ultimate performance of a receiver. In a hard-limiting transponder (see Figure 9d), $(j + \text{IM})/S$ is usually a factor of four (or 6-dB) worse than the input J/S, when J is large compared to S and the jammer is a CW [17]. These types of standard analysis results are easily confirmed with the IM Microscope.

Note that if computations of power division can be run without the need for spectral plots (Fourier transforms), there will be a significant savings in run time and computer memory.

IM Microscope results with nonrandomized input signals

The simulation aspects of the new algorithm present many challenges which have not yet been thoroughly explored. While most commonly used signals in satellite systems are automatically orthogonal in the sense of frequency difference or information content, they are not necessarily statistically independent. Thus, two digital signals originating in the same earth station may be transmitted at different center frequencies but in bit sync. These signals will not have the same intermod spectrum as two digital signals whose bit streams are out of sync or that have incommensurate bit periods. Analytical approaches in the literature always assume that the signals are statistically independent. In this case, obtaining the spectrum of a harmonic involves the convolution of spectra from the fundamental components. The IM Microscope, on the other hand, always finds the spectrum that would be measured in a laboratory situation under rigorously identical input signal conditions, regardless of the statistical independence or non-independence of the inputs.

As an example of the spectrum obtained with nonrandomized signals, Figure 14 shows a two-carrier ED/CW input/output IM Microscope plot with a single signal block used in the computation. The triangular ED signals are synchronized and of equal amplitude. In contrast to Figure 7, where the triangular waveshapes are randomized and block averaging is used, none of the intermod spectrum components spread out, even at the higher harmonics. This result should not be interpreted as wrong, since it is the correct answer when the ED waveforms are synchronized, and would be observed in a laboratory measurement under identical conditions.

Conclusions

A new procedure for solving for intermod distortion in satellite systems has been developed at COMSAT and used in a number of applications. The IM Microscope has several attributes which set it apart from other methods—in particular its ability to solve for the intermod waveform directly, by a process of elimination. It can employ an arbitrary nonlinearity and, unlike previous approaches, does not depend on a series expansion. This procedure has been used to resolve practical satellite engineering problems that could not have been completed in any other way.

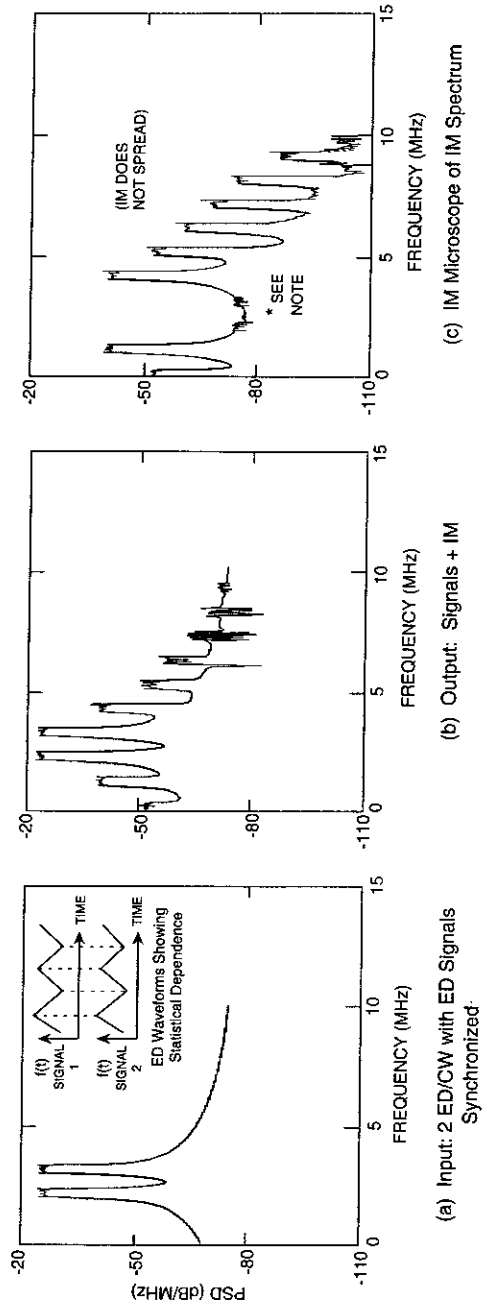

*NOTE: These figures were created with a test version of the IM microscope that contained a minor error in calculation λ_1 and λ_2, resulting in a small residual component of the original signals, S_1 and S_2.

Figure 14. *IM With Statistically* Dependent *Sawtooth ED Signals*

Acknowledgments

The authors would like to thank COMSAT World Systems for its support and funding of the work reported herein. S. J. Campanella's recommendations for revision of the original manuscript, and his careful proofreading, were very helpful. C. Pike, who used the IM Microscope in his work while at COMSAT [3], first demonstrated its use with filtered noise, tested various windowing functions, and contributed Figures 12 and 13. J. Lee used the IM Microscope while at COMSAT [4], and added to the memory capability of the original program by porting it to a new FORTRAN compiler, adding new graphics, and, with I. Brelian, adding the QPSK DSSS signal model.

References

[1] O. Shimbo, "Effects of Intermodulation, AM-PM Conversion and Additive Noise in Multicarrier TWT Systems," *Proc. IEEE*, Vol. 59, No. 2, February 1971, pp. 230–238.

[2] J. C. Fuenzalida, O. Shimbo, and W. L. Cook, "Time-Domain Analysis of Intermodulation Effects Caused by Nonlinear Amplifiers," *COMSAT Technical Review*, Vol. 3, No. 1, Spring 1973, pp. 89–143.

[3] D. Arnstein, C. Pike, and G. Estep, "On-Board AJ Enhancement Using Adaptive Nonlinear Processing: Practical Aspects of Smart AGC™ Implementation," IEEE Military Communications Conference (MILCOM '92), San Diego, CA, October 1992, *Conf. Rec.*, Vol. 1, pp. 7.5.1–7.5.7.

[4] D. Arnstein and J. W. Lee, "AJ Performance of Smart AGC™ in MILSATCOM Networks: A Review of Space System Design Principles and Applications," AIAA 14th International Communications Satellite Systems Conference, Washington, D.C., March 1992, *Conf. Rec.*, pp. 23–31.

[5] D. Arnstein, "Power Division on Spread Spectrum Systems with Limiting," *IEEE Transactions on Communications*, Vol. COM-27, No. 3, March 1979, pp. 574–582.

[6] C. W. Helstrom, *Statistical Theory of Signal Detection*, Oxford, England: Pergamon Press, 1968, Ch. 2.

[7] A. V. Oppenheim and R. W. Schafer, *Digital Signal Processing*, Englewood Cliffs, New Jersey: Prentice-Hall, 1975, Ch. 3.

[8] W. B. Davenport and W. L. Root, *An Introduction to the Theory of Random Signals and Noise*, New York: McGraw-Hill, 1958, Ch. 13, "Introduction to the Transform Method."

[9] N. Blachman, "Detectors, Bandpass Nonlinearities, and Their Optimization: Inversion of the Chebyshev Transform," *IEEE Transactions on Information Theory*, Vol. IT-17, No. 4, July 1971, pp. 398–404.

[10] A. Berman and C. Mahle, "Nonlinear Phase Shift in Traveling Wave Tubes as Applied to Multiple Access Communications Satellites," *IEEE Transactions on Communication Technology*, Vol. 18 , No. 1 , February 1970, pp. 37–48.

[11] R. W. Hornbeck, *Numerical Methods*, New York: Quantum Publishers, 1975.

[12] R. G. Lyons, "Stochastic Analysis of Signal Sharing in a Bandpass Nonlinearity," *IEEE Transactions on Communications*, Vol. COM-22, No. 11, November 1974, pp. 1778–1788.

[13] N. M. Blachman, "The Signal X Signal, Noise X Noise, and Signal X Noise Output of a Nonlinearity," *IEEE Transactions on Information Theory*, Vol IT-14, No. 1, January 1968, pp. 21–27.

[14] D. Middleton, *An Introduction to Statistical Communication Theory*, Los Altos, California: Peninsula Publishing, 1987, p. 624.

[15] R. J. F. Fang and W. A. Sandrin, "Carrier Frequency Assignment for Nonlinear Repeaters," *COMSAT Technical Review*, Vol. 7, No. 1, Spring 1977, pp. 227–245.

[16] X. T. Vuong *et al.*, "Some Practical Strategies for Reducing Intermodulation in Satellite Communications," *IEEE Transactions on Aerospace and Electronic Systems*, Vol. 24, No. 6, November 1988, pp. 755–765.

[17] C. Cahn, "A Note on Signal to Noise in Band Pass Limiters," *IRE Transactions on Information Theory*, Vol. 7 , No. 1 , January 1961, pp. 39–43.

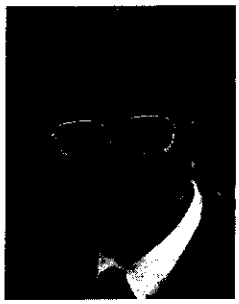

Donald S. Arnstein received a B.S.E.E. (magna cum laude) from City College of New York in 1962; Master's and Professional Engineer's degrees from the Massachusetts Institute of Technology in 1963 and 1967, respectively; and a Ph.D. from the University of California, Los Angeles, in 1972. He joined COMSAT in 1979 and is currently Manager of the Satellite Systems Department in the Microwave Technology and System Division at COMSAT Laboratories, where he provides systems analysis and design support for international, domestic, military, and mobile satellite systems. Dr. Arnstein is a Senior Member of IEEE; past Secretary of the Satellite and Space Communications Subcommittee of the IEEE Communications Society; past Chairman of the Washington, D.C., chapter of the IEEE Communications Society; and a member of Tau Beta Pi, Eta Kappa Nu, and Sigma Xi engineering honor societies.

Xuyen T. Vuong obtained his B.S.E.E., M.Eng., and Ph.D. from California State University, Carleton University, and the University of Western Ontario, respectively. He received United States AID Scholarships during his undergraduate study, and Ontario Graduate Fellowships during his graduate study. He also taught and conducted research as a Postdoctoral Fellow and an Assistant Professor at the University of Ottawa and Concordia University.

Dr. Vuong has held various science, engineering, and management positions at COMSAT Laboratories and COMSAT Systems Division, GTE Spacenet, Telesat Canada, Canadian Astronautics and Spar Aerospace, and cofounded Systar Telecommunications. Currently, he is a Staff Engineer at Science Applications International Corporation (SAIC), performing systems engineering and analysis on future military satellite communications systems. He has published more than 40 journal and conference papers on satellite communications, optimization techniques, and state estimation and control, and is a Senior Member of IEEE.

Calvin B. Cotner received a B.S. in electrical engineering (cum laude) from Princeton University in 1962, and an M.S.E.E. from Cornell University in 1964. He has been with COMSAT since 1967 and is currently Director of Technical Liaison and Analysis with COMSAT World Systems. His primary technical interests are earth station design, transmission analysis, and high-power amplifiers. He has held several technical management positions in COMSAT Laboratories, COMSAT General, and COMSAT World Systems, including representing the U.S. Signatory on the INTELSAT Board of Governors' Technical Advisory Committee for 5 years. He is a colonel in the Signal Corps, U.S. Army Reserve, and a Commandant's List Graduate of the U.S. Army Command and General Staff College. He is a Senior Member of AIAA.

Haresh M. Daryanani received a B.S.E.E. with Honors from Old Dominion University in 1987. As a member of the Systems Analysis Department in COMSAT Systems Division (CSD), he provided systems engineering support for the design and integration of turnkey earth terminal systems, including earth terminal specifications and overall end-to-end network analyses. As a member of CSD's Firmware Engineering Department, he was responsible for developing and testing DSP and microprocessor code resident in Inmarsat-M/B maritime communications networks. Prior to joining COMSAT in 1988, he served as a research assistant in the Instrument Research and Flight Electronics Divisions at NASA's Langley Research Center.

Mr. Daryanani is currently a Staff Engineer with the Defense Information Systems Agency in Reston, Virginia. He is a member of IEEE and the Eta Kappa Nu and Tau Beta Pi engineering honor societies.